

Cluster galaxies in XMMU J2235-2557: galaxy population properties in most massive environments at $z \sim 1.4$ *

V. Strazzullo¹, P. Rosati², M. Pannella¹, R. Gobat³, J. S. Santos⁴, M. Nonino⁴, R. Demarco⁵, C. Lidman⁶, M. Tanaka^{2,7}, C. R. Mullis⁸, C. Nuñez², A. Rettura⁹, M. J. Jee¹⁰, H. Böhringer¹¹, R. Bender^{11,12}, R. J. Bouwens^{13,14}, K. Dawson¹⁵, R. Fassbender¹¹, M. Franx¹³, S. Perlmutter¹⁶, and M. Postman¹⁷

¹ National Radio Astronomy Observatory, 1003 Lopezville Rd., Socorro, NM 87801, USA
e-mail: vstrazzu@nrao.edu

² European Southern Observatory, Karl Schwarzschild Strasse 2, 85748 Garching bei Muenchen, Germany

³ CEA, Laboratoire AIM-CNRS-Université Paris Diderot, Irfu/Sap, Orme des Merisiers, 91191 Gif-sur-Yvette, France

⁴ INAF-Osservatorio Astronomico di Trieste, via Tiepolo 11, 34131 Trieste, Italy

⁵ Department of Astronomy, Universidad de Concepción, Casilla 160-C, Concepción, Chile

⁶ Australian Astronomical Observatory, PO Box 296, Epping, NSW 1710, Australia

⁷ Institute for the Physics and Mathematics of the Universe, The University of Tokyo, 5-1-5 Kashiwanoha, Kashiwa-shi, Chiba 277-8583, Japan

⁸ Wells Fargo Bank, 4525 Sharon Road, Charlotte, NC 28211, USA

⁹ Department of Physics and Astronomy, University of California, Riverside, CA 92521, USA

¹⁰ Department of Physics, University of California, Davis, One Shields Avenue, Davis, CA 95616, USA

¹¹ Max-Planck-Institut für Extraterrestrische Physik, Giessenbachstrasse, 85748 Garching, Germany

¹² Universitäts-Sternwarte, Scheinerstrasse 1, Munich 81679, Germany

¹³ Leiden Observatory, Leiden University, PO Box 9513, 2300 RA Leiden, The Netherlands

¹⁴ Astronomy Department, University of California, Santa Cruz, CA 95064, USA

¹⁵ Department of Physics and Astronomy, University of Utah, Salt Lake City, UT 84112, USA

¹⁶ Lawrence Berkeley National Laboratory, 1 Cyclotron Rd., Berkeley, CA 94720, USA

¹⁷ Space Telescope Science Institute, 3700 San Martin Drive, Baltimore, MD 21218, USA

Received 21 June 2010 / Accepted 29 August 2010

ABSTRACT

We present a multi-wavelength study of galaxy populations in the core of the massive, X-ray luminous cluster XMMU J2235 at $z = 1.39$, based on high quality VLT and HST photometry at optical and near-infrared wavelengths.

We derive luminosity functions in the z , H , and K_s bands, approximately corresponding to restframe U , R and z band. These show a faint-end slope consistent with being flat, and a characteristic magnitude M^* close to passive evolution predictions of M^* of local massive clusters, with a formation redshift $z > 2$.

The color–magnitude and color–mass diagrams show evidence of a tight red sequence (intrinsic scatter ≤ 0.08) of massive galaxies already in place, with overall old stellar populations and generally early-type morphology. Beside the red colors, these massive ($> 6 \times 10^{10} M_\odot$) galaxies typically show early-type spectral features, and rest-frame far-UV emission consistent with very low star formation rates ($SFR < 0.2 M_\odot \text{ yr}^{-1}$).

Star forming spectroscopic members, with SFR of up to $\sim 100 M_\odot/\text{yr}$, are all located at clustercentric distances ≥ 250 kpc, with the central cluster region already appearing effectively quenched. Most part of the cluster galaxies more massive than $6 \times 10^{10} M_\odot$ within the studied area do not appear to host significant levels of star formation.

The high-mass end of the galaxy populations in the core of this cluster appears to be in a very advanced evolutionary stage, not only in terms of formation of the stellar populations, but also of the assembly of the stellar mass. The high-mass end of the galaxy stellar mass function is essentially already in place. The stellar mass fraction estimated within r_{500} ($\sim 1\%$, Kroupa IMF) is already similar to that of local massive clusters.

On the other hand, surface brightness distribution modeling of the massive red sequence galaxies may suggest that their size is often smaller than expected based on the local stellar mass vs. size relation. An evolution of the stellar mass vs. size relation might imply that, in spite of the overall early assembly of these sources, their evolution is not complete, and processes like minor (and likely dry) merging might still shape the structural properties of these objects to resemble those of their local counterparts, without substantially affecting their stellar mass or host stellar populations. Nonetheless, a definite conclusion on the actual relevance of size evolution for the studied early-type sample is precluded by possible systematics and biases.

Key words. galaxies: clusters: individual: XMMU J2235.3-2557 – galaxies: evolution – galaxies: high-redshift – galaxies: luminosity function, mass function – galaxies: fundamental parameters

* Based on observations made with the NASA/ESA Hubble Space Telescope under Program IDs 10698, 10496, and 10531, and with the Very Large Telescope at the ESO Paranal Observatory under Program

IDs 60.A-9284, 072.A-0706, 073.A-0737, 074.A-0023, 077.A-0177, 077.A-0110, 079.A-0758, and 081.A-0759.

1. Introduction

Galaxy clusters at high redshift provide us with a unique yet rare chance to investigate the effect of the highest density environments on the evolution of galaxy populations. Due to the extreme rarity of massive galaxy clusters, and especially more so at early cosmic epochs, even wide-area deep surveys do not probe these peculiar environments which thus need to be searched and identified in specifically designed surveys, and then followed-up with observations across a wide range of wavelengths in order to maximize the scientific return of their discovery.

Thanks to considerable efforts with on-going cluster surveys, which are utilizing a variety of methods (e.g., Gladders & Yee 2000; Rosati et al. 2002; Eisenhardt et al. 2004; Wilson et al. 2005; Wittman et al. 2006; Fassbender 2008; Staniszewski et al. 2009; Andreon et al. 2009; Demarco et al. 2010, and references therein), the number of known high-redshift clusters is increasing, however only a handful of spectroscopically confirmed galaxy clusters beyond redshift 1.3 have been discovered to date (Mullis et al. 2005; Stanford et al. 2005, 2006; Eisenhardt et al. 2008; Wilson et al. 2009; Papovich et al. 2010; Tanaka et al. 2010).

Galaxy clusters at such high redshifts are not only important for studying the emergence of the large scale structure and for constraining cosmological models, but also specifically for the evolution of massive early-type galaxies which seem to dominate massive cluster galaxy populations even beyond redshift one. The further back in cosmic time we can reach, and thus the closer we can get to the major stages of the galaxy formation process, the tighter are the constraints we can set on the evolution of these galaxies, as well as on the relevance of the cluster environment in shaping their physical properties (among many others, Toft et al. 2004; Blakeslee et al. 2006; Andreon 2006; Strazzullo et al. 2006; De Propriis et al. 2007; De Lucia et al. 2007; Kodama et al. 2007; Holden et al. 2007; Zirm et al. 2008; Andreon 2008; Lidman et al. 2008; Gobat et al. 2008; Muzzin et al. 2008; Rettura et al. 2010; Mei et al. 2009; Collins et al. 2009; Hilton et al. 2009; Rosati et al. 2009, and references therein).

While the detailed study of galaxies with stellar masses $M \lesssim 10^{10} M_{\odot}$ is still limited at $z > 1$, even with the current generation of 10 m class telescopes, massive galaxy populations can be studied out to high redshift in sufficient detail, in terms of their structure, star formation histories, and stellar masses. These studies allow us to constrain the evolution of massive galaxies in more nuances than the old, and now widely superseded in its original form, “monolithic vs. hierarchical” question. This provides valuable input to theoretical modeling of galaxy evolution, the detailed comparison of cluster and field galaxies being one of the many examples (Menci et al. 2008; Romeo et al. 2008).

Taking advantage of the full range of available observations, across the widest possible range of cosmic epochs and environments, has become particularly important in order to probe different aspects of galaxy evolution, and to test specific predictions of theoretical models. As an example, the introduction of various forms of so-called feedback mechanisms to modulate galaxy evolution has reconciled previously considered “anti-hierarchical” observations with hierarchical predictions (e.g., De Lucia et al. 2006; Bower et al. 2006, and references therein), and elucidated the decoupling between star formation and mass assembly histories of massive galaxies. In order to probe these two processes independently, galaxy evolution has to be studied by directly sampling galaxy populations up to the highest redshifts.



Fig. 1. A color image of XMMU J2235 obtained by combining the ACS F775W and F850LP and NICMOS F160W images (*North is up, East to the left*). The image shows a region of about 2×2 arcmin², corresponding to about 1×1 Mpc² at the cluster redshift.

In this work we present multi-wavelength observations of the X-ray luminous galaxy cluster XMMU J2235-2557 (Mullis et al. 2005, hereafter XMMU J2235, RA = $22^{\text{h}}35^{\text{m}}20^{\text{s}}.82$, Dec = $-25^{\circ}57'40.3''$, J2000) at $z = 1.39$, which is the most massive virialized structure discovered beyond redshift one (Jee et al. 2009; Rosati et al. 2009), spectroscopically confirmed with 30 cluster members with redshift in the range $1.37 < z < 1.41$. This is a follow-up work of the first multi-wavelength analysis presented in Rosati et al. (2009), which uses an enhanced data set and is aimed at obtaining a more comprehensive picture on the star formation, stellar mass distribution, and morphological structure of the galaxy populations in the cluster central regions.

Throughout this paper, we adopt a $H_0 = 70 \text{ km s}^{-1} \text{ Mpc}^{-1}$, $\Omega_M = 0.3$, $\Omega_{\Lambda} = 0.7$ cosmology, and the *AB* magnitude system.

2. Data and derived quantities

2.1. Observations and catalog production

This work is based on a multi-wavelength dataset collected in the field of XMMU J2235 with the VLT and HST in the wavelength range 3500 \AA to $2 \mu\text{m}$. In the following we use VLT photometry (VIMOS *U*, FORS2 *R*, HAWK-I *J* and *K_s*) and spectroscopy (FORS2), and HST photometry (ACS F775W and F850LP – hereafter *i* and *z*, and NICMOS F160W – hereafter *H*). A description of the first available HST/ACS data and VLT spectroscopic campaign has been published in Rosati et al. (2009); in this work we use the full presently available ACS dataset, including images from program GO-10496 (Dawson et al. 2009), as was presented in Jee et al. (2009). VLT/HAWK-I data have been published in Lidman et al. (2008), while VLT/FORS2 imaging was presented in Mullis et al. (2005), thus we refer to these papers for a full description of these observations.

The NICMOS F160W data we used in this work were obtained in August 2008 (GO 14, Proposal ID 10531, PI: Mullis), resulting in a mosaic of about 2.5×2.5 arcmin² with an average exposure time of ~ 1 h.

Table 1. Summary of the imaging data used in this work.

Telescope/Instrument	Filter	<i>FWHM</i> (arcsec)	Area (total/used) (arcmin ²)
VLT/VIMOS	<i>U</i>	0.8	50/10.3
VLT/FORS2	R_SPECIAL	0.75	50/10.3
HST/ACS	<i>F775W</i>	0.1	11/10.3
HST/ACS	<i>F850LP</i>	0.1	11/10.3
VLT/HAWK-I	<i>J</i>	0.55	180/10.3
HST/NICMOS	<i>F160W</i>	0.35	6.2/6.2
VLT/HAWK-I	<i>K_s</i>	0.4	180/10.3

Notes. Columns 1 and 2 list the instruments and filters with which images were acquired. Column 3 gives an estimate of the image resolution. Column 4 gives the total area of the image/mosaic in each passband, and the actual area used to build the multi-wavelength catalog. Further details about these images, and additional information specific to their use for different purposes in this work, are given in the text.

The *U* band data (ESO 079.A-0758, PI: Nonino) were obtained in August 2007 with VIMOS at the VLT. 32 dithered observations were collected for a total of 6 h 20 m with seeing conditions ranging from 0.5 to 1.2. The images were reduced and stacked in a similar fashion to Nonino et al. (2009). The zero point of the mosaic was derived using standard stars observed in photometric nights. The limiting magnitude of the mosaic covering the cluster was estimated from the counts distribution in a 2'' aperture¹ centered on 5000 random points. After correcting for aperture effects (0.19 mag), and for the effect of the correlation in the noise introduced by the coaddition step (0.2 mag), the final value is 28.8 AB mag (1σ).

Source extraction and photometry were performed with SExtractor (Bertin & Arnouts 1996), either in single-image (for the determination of MAG_AUTOs used for deriving the luminosity functions) or in dual-image mode (for the determination of aperture colors used for deriving the broad-band SEDs). We adopted MAG_AUTO as an estimate of total magnitude, while colors (and thus the broad-band SEDs) were estimated in apertures of 1'' and 1.5''. These aperture sizes were chosen based on the typical angular size of galaxies at the redshift we are interested in, and on the resolution of the available data. The 1'' apertures allow us to measure colors of cluster members within 1–2 effective radii (see Sect. 4), while for estimating stellar masses we used the 1.5'' apertures as a compromise between optimising the *S/N*, minimising the effect of neighbors, and reducing the errors on the correction to total masses (see Sect. 2.3).

The angular resolution of our imaging data ranges from a *FWHM* of $\sim 0.1''$ for the ACS images to $\sim 0.8''$ for ground-based optical images (see Table 1). In order to match these different resolutions in the multicolor photometric catalog, aperture corrections were applied in each passband as estimated from the growth-curve of point-like sources in the field (similar to the approach described in e.g. Rettura et al. 2006). This resolution-matching approach allows us to measure accurate photometry without degrading the image quality in any of the passbands, which is an important advantage when dealing with a crowded field such as a cluster core².

¹ Here and in the following, aperture sizes refer to the aperture diameter.

² For aperture sizes used in this work, and for our worse resolution of $\sim 0.8''$, we estimate through simulation of synthetic sources (with the IRAF task mkobjects) that this resolution-matching approach corrects for systematics of 0.1 to 0.5 mag (depending on the aperture size), with a residual systematic offset of 0.01–0.04 mag for a de Vaucouleurs

Magnitudes were corrected for Galactic extinction according to Schlegel et al. (1998).

Multi-wavelength photometric and morphological catalogs for the available sample of ~ 30 spectroscopically confirmed cluster members will be published in a forthcoming paper (Nuñez et al., in prep.).

2.2. Photometric redshifts

We used the *U*, *R*, *i*, *z*, *J*, *H*, *K_s* photometric coverage of the XMMU J2235 field, to estimate photometric redshifts (photo-*z*s) by comparing the observed photometry with a library of 33 SED templates covering a range of star-formation histories, ages and dust content. Together with local galaxy templates (e.g., Coleman et al. 1980; Mannucci et al. 2001; Kinney et al. 1996), we used a set of semi-empirical templates based on observations plus fitted SED models (Maraston 1998; Bruzual & Charlot 2003) of ~ 300 galaxies in the FORS Deep Field (Heidt et al. 2003) and Hubble Deep Field (Williams et al. 1996), in order to better represent objects to higher redshifts. A different prior on the redshift distribution is assumed for different types of templates (e.g. an old local elliptical template is assumed to be increasingly unlikely at higher redshifts, while templates corresponding to young stellar populations or QSOs are assumed to have a basically flat likelihood across the whole redshift range probed). In addition, a weak broad prior on the absolute optical and NIR magnitude lowers the probability to have magnitudes brighter than -25 and fainter than -13 . Ly- α forest depletion of galaxy templates is implemented according to Madau (1995). The “best-fit” photo-*z* z_{phot} is chosen as the redshift maximizing the probability among all templates, and an error on z_{phot} is defined as $e_{z_{\text{phot}}} = [\sum_{ij}(z_i - z_{\text{phot}})^2 P_{ij}]^{1/2}$, with z_i the considered redshift steps, and P_{ij} the contribution of the *j*th template to the total probability function at redshift z_i . We refer to Bender et al. (2001); Gabasch et al. (2004); Brimiouille et al. (2008) for a detailed description of both the photo-*z* estimation method, and the construction of the templates.

Systematic offsets between the measured and template-predicted colors as a function of redshift (which may be due for instance to errors in the estimated zero-point and aperture corrections, uncertainties in the filter response curves, or systematics in the templates) were estimated using ~ 70 spectroscopic redshifts available within the $\sim 3' \times 3'$ field, and corrected for in order to minimize the systematic shift between observed and predicted colors for well-fitted spectroscopic galaxies.

The photo-*z* performance against the available spectroscopic sample is shown in the top panel of Fig. 2. The figure clearly shows the impact of the lack of coverage between the *U* and *R* passbands at lower redshifts, in particular at $z \lesssim 0.6$ where the 4000 Å break is poorly sampled by the available photometric coverage, often resulting in unconstrained, inaccurate photo-*z*'s. However, by comparison with a spectroscopic sample of ~ 50 objects in the redshift range $1 < z < 2$ ($\sim 40\%$ of these are cluster members), we estimate a systematic offset (median $\Delta z/(1+z)$) of 0.006, a scatter of $\Delta z/(1+z) < 6\%^3$, and 4% catastrophic outliers (two objects with $|\Delta z/(1+z)| \geq 20\%$; we

profile with effective radius 0.24'' (~ 2 kpc at $z = 1.39$, about the median effective radius of our red-sequence sample), and ~ 0.05 mag for effective radii of 1.2'' (~ 10 kpc at $z = 1.39$, about our largest effective radius), and a scatter of about 0.01–0.02 mag.

³ The NMAD estimator (Hoaglin et al. 1983; Ibert et al. 2009) gives a scatter of 0.045 for the whole spectroscopic sample, and 0.03 in the range $1 < z < 2$.

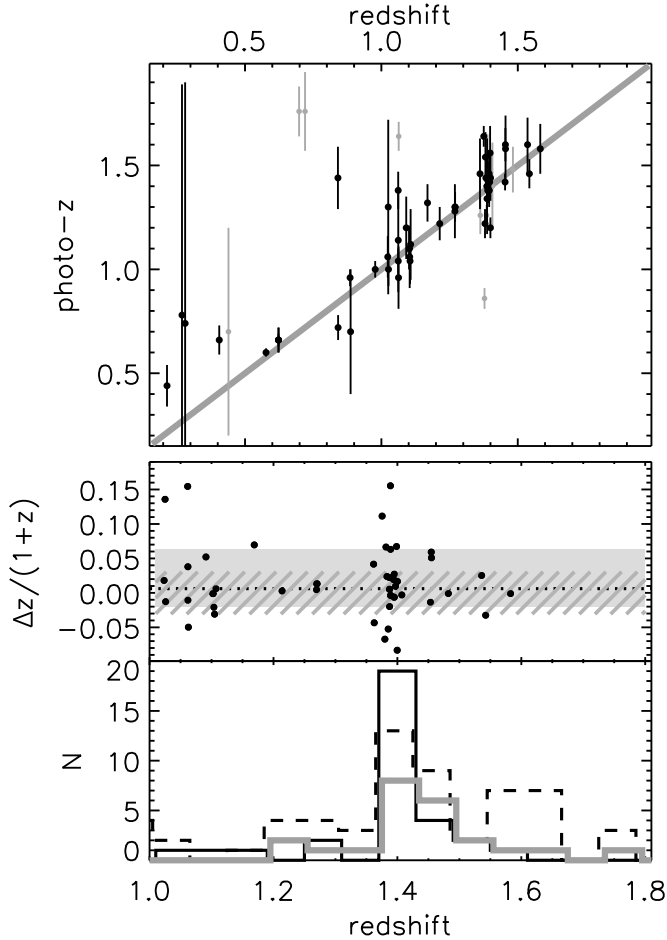


Fig. 2. *Top panel:* photometric vs. spectroscopic redshifts for the whole spectroscopic sample within the considered field (one point at $z = 3.26$ with $\text{photo-}z = 3.44$ is not plotted). The gray line traces the bisector. Gray symbols show uncertain spectroscopic redshifts (quality flag B or worse, see Rosati et al. 2009; these objects are plotted together with the secure redshifts in the lower panels). *Middle panel:* $\Delta z/(1+z)$ as a function of redshift for the spectroscopic sample at $1 < z < 2$ (one catastrophic outlier with an (uncertain) redshift $z = 1.06$ and a $\text{photo-}z = 1.64$ falls out of the plot). The dotted line and the gray shaded area show the median and the 16th–84th percentile range of $\Delta z/(1+z)$. The hatched area shows the $\Delta z/(1+z)$ scatter as estimated by the NMAD estimator. *Bottom panel:* the spectroscopic (solid black line) and photometric (dashed line) redshift distribution of bright ($H < 22.2$) galaxies in the studied field. The gray histogram shows instead the photometric redshift distribution of all spectroscopic cluster members. Histograms are slightly offset for clarity.

note that both sources have a spectroscopic redshift deemed uncertain, with a quality flag B or worse, see Rosati et al. 2009). The middle panel of Fig. 2 shows in more detail the photo- z performance in the $1 < z < 2$ range, suggesting that in the relevant redshift range we can derive accurate enough photo- z s⁴. In the bottom panel of Fig. 2 we compare the spectroscopic (solid black line) and photometric (dashed line) redshift distributions in this redshift range for bright galaxies ($< M^* + 1$), where we have enough spectroscopic coverage (see below, also figures in Sect. 4). While the peak at the cluster redshift is also visible in

⁴ Out of 7 catastrophic failures over the whole $0 < z < 3.5$ redshift range, four have an uncertain spectroscopic redshift, and two are $z \sim 0.3$ sources for which the photo- z is essentially unconstrained, as the errorbars in Fig. 2 show.

the photo- z distribution, the gray histogram shows the spread in photo- z s of all available spectroscopic members (regardless of their magnitude).

By comparison with the available spectroscopic sample, we estimate that by selecting photo- z candidates within 3σ of the cluster redshift ($1 < z < 1.8$) we include all spectroscopic members, while slightly more than half of the selected sources are interlopers (94% of which in the range $1 < z_{\text{spec}} < 1.8$)⁵.

2.3. Stellar masses

Stellar masses were obtained by fitting Bruzual & Charlot (2003) models to the (resolution-matched) U, R, i, z, J, H, K_s SEDs as measured in $1.5''$ apertures (as described in e.g., Gobat et al. 2008; Rosati et al. 2009). Stellar masses are determined for models of fixed solar metallicity and with a Salpeter (1955) IMF, however for the purpose of comparison with other literature samples (see below) stellar masses are converted to Kroupa (2001) IMF masses⁶. Different determinations of the stellar masses were derived, using different star formation histories (exponentially declining, delayed exponentially declining, with or without a recent burst of star formation), including or not dust attenuation. These different determinations mostly agree within better than 50%, (the scatter between different determinations is about $\sim 30\%$), and never differ by more than a factor of two. We will consider this $\sim 30\%$ scatter as an estimate of the typical error on the stellar masses due to different SFHs and dust properties, however we remind the reader that this estimate does not include other systematics, including those due to IMF and metallicity being different from what we assumed.

In order to obtain total stellar masses, the masses derived from the SEDs measured within a radius of $0.75''$ were renormalized by the flux ratio between the $1.5''$ aperture magnitude and the total (MAG_AUTO) magnitude in the z band. This approximation neglects the effects of a change in stellar mass-to-light ratio in the very external regions of the galaxies. However, given the typical galaxy sizes, the correction is generally small: among the sample relevant to this work ($1 < z < 2$, $\log(M_*/M_\odot) > 10.4$), the median correction is less than 10%, and for the great part of the sources is less than 50%. We thus expect this error not to significantly affect our results, also in view of the uncertainties generally affecting SED-determined stellar masses (e.g., Longhetti & Saracco 2009).

2.4. Structural properties

We used the GALFIT (Peng et al. 2002) software to model surface brightness profiles of sources brighter than $z \sim 24.2$. We set this magnitude limit based on S/N considerations, according to previous results on the accuracy of the retrieved parameters as a function of magnitude (S/N) from simulations of surface brightness fitting (e.g., among others, Ravindranath et al. 2006; Pannella et al. 2009b, see also below), as well as visual

⁵ While the 3σ photo- z retained samples are used to include all plausible cluster members, for the purpose of statistical analysis (as for instance in Sect. 6), in the following we also use 2σ photo- z retained samples. Based on the comparison with the spectroscopic sample, these too are estimated to be virtually 100% complete, and affected by an almost 50% contamination by interlopers. In the stellar mass range relevant to this work ($M > 10^{10} M_\odot$), the difference between the two samples is just ~ 10 sources, with almost 90% of the 3σ sample belonging to the 2σ sample as well.

⁶ $\text{Log}(\text{Mass}_{\text{Kroupa}}) = \text{Log}(\text{Mass}_{\text{Salpeter}}) - 0.19$.

morphology (Postman et al. 2005). This is sufficient to probe the morphologies of red galaxies in XMMU J2235 down to $\sim M^* + 1$.

We fitted PSF-convolved Sersic (1968) profiles to ACS z band images, using the PSF models derived from principal component analysis (Jee et al. 2007, 2009); using a stack of high S/N , unsaturated point-like sources in the field does not change our results. The possibility offered by GALFIT to simultaneously fit multiple sources is particularly useful in a cluster environment: when fitting a galaxy surface brightness, all nearby sources⁷ brighter than $\text{mag}_{\text{galaxy}} + 3$ were also modeled at the same time, reducing biases produced by contamination by neighbors.

A detailed description of the morphological properties of bright cluster galaxies, and a comprehensive morphological analysis including the high-resolution ground-based NIR data, will be presented in Nuñez et al. (in prep.). In the following we only use the Sersic index n_{Sersic} to broadly classify galaxies in early and late morphological types, and the estimated (circularized) effective radius as an estimate of the galaxy size.

3. Luminosity functions

The luminosity function (LF) of galaxies in the central region of XMMU J2235 was determined in three passbands (z , H , K_s), roughly corresponding to restframe U , R , and z bands. The regions actually used for the LF determination were about 7.5, 6, and 7 arcmin², in the z , H , and K_s bands, respectively. At the cluster redshift, the area probed extends out to a clustercentric distance of about 700 kpc. The completeness limits of the z , H , and K_s band images were estimated based on the turnover of the number counts of sources with $S/N > 10$, and turn out to be ~ 25.3 , 25, and 23, respectively.

For the purpose of statistical subtraction of background contamination, we also made use of publicly available photometry acquired with the same, or very similar, instrument/filter as the XMMU J2235 images. For the K_s band we used VLT/ISAAC K_s band photometry in a ~ 60 square arcmin region within the GOODS CDF-S field (v2.0 release, Retzlaff et al. 2010). Only regions with a 10σ depth comparable or better than the XMMU J2235 K_s image were used. For the H band we used the NICMOS imaging on a ~ 5 arcmin² region in the Hubble Ultra Deep Field (Thompson et al. 2005), while for the z band we used ACS photometry in the GOODS (North and South) fields (v2.0 release, Giavalisco et al. 2004; Giavalisco et al., in prep.), for an overall area of more than 200 arcmin².

For all fields, point-like sources were identified and removed based on the combination of morphological/concentration parameters estimated by SExtractor (MAG_AUTO, FLUX_RADIUS, CLASS_STAR, FWHM_IMAGE) on the z band image.

Luminosity functions (LFs) were determined by means of statistical background subtraction, but at the same time taking full advantage of the available spectroscopic and photometric redshift information. The best purely statistical approach would avoid binning the data, and would derive the cluster galaxy LF by simultaneously modeling the number counts in the cluster and in a control field, as described in detail in Andreon et al. (2005). However, this approach would not allow us to take into account the information about cluster membership that we derive by other means (spectroscopic and photometric redshifts).

While information on cluster membership is obviously always relevant, its specific importance in the determination of the LF (and its errors) depends on different factors including the quality of such membership information and how much it contributes to the constraints on the LF. When only one cluster field is available, the statistics at the LF bright end is very poor; furthermore, particularly in the case of very distant clusters, the imaging depth can reach at most about 3–4 mag fainter than M^* . In these conditions, it is very important to make full use of all the available information, in order to best constrain the LF even when the intrinsically low counts would make its purely statistical determination relatively loose.

We thus adopted the following approach (which extends with the use of photo- z s the approach adopted in Strazzullo et al. 2006): we first determined the LF in each passband by subtracting the (area normalised) counts in the control field from the counts in the cluster field. The error on the excess counts was determined by summing in quadrature the Poissonian errors⁸ from both cluster and field counts (even though it is dominated by the cluster contribution when the cluster field is much smaller than the control field). The error contribution coming from cosmic variance due to galaxy clustering, as estimated according to Huang et al. (1997), is much smaller than the Poisson error (a factor of a few percent at most) and was neglected (see also e.g., Andreon et al. 2005; Strazzullo et al. 2006).

We then took into account the spectroscopic information, imposing that in each magnitude bin the excess counts are at least equal to the spectroscopic members in that bin. The spectroscopic (and photo- z) information is also considered in the determination of the final error on the excess counts in each bin. The membership for the brightest galaxy populations in the core of XMMU J2235 can be considered quite well established (see also figures in Sect. 4 below). In the critical (for the LF determination) range from the BCG magnitude to M^* , the spectroscopic completeness is about 70%. Furthermore, basically all plausible members brighter than M^* were targeted for spectroscopic follow-up, and thus the remaining sources without spectroscopic redshift have a photo- z far below the cluster redshift, and well beyond 3σ from the cluster redshift according to the photo- z estimated rms. Therefore, in estimating the error on the excess counts, we assumed that: i) when all objects in a magnitude bin have a spectroscopic redshift, or a photo- z beyond 3σ from the cluster redshift, the LF is basically “membership determined” without the error contribution from the background counts; ii) the lower limit on the excess counts cannot go below the lower limit based on the spectroscopic excess counts; and iii) the upper limit on the excess counts is limited by the upper limit on the counts of spectroscopic members plus photo- z candidate members within 3σ from the cluster redshift. We remind the reader that the 3σ photo- z retained sample is estimated to be 100% complete, and affected by a $\geq 50\%$ contamination, thus we expect the upper limits based on such sample to be robust.

In Fig. 3 we show the binned LFs determined in this way in the three z , H , and K_s passbands. The available photometry reaches out to $\sim M^* + 2$ or $M^* + 4$ depending on the passband. For ease of comparison, all LFs are plotted in Fig. 3 over a magnitude range of about 5 mag, from $\sim M^* - 2$ to $\sim M^* + 3.5$. The formal best-fit Schechter (1976) function determined by χ^2 minimization on the binned counts plotted, with errors as described above, is also shown. For the H band we plot both the

⁷ Sources within a region of dimensions about 4 times the dimension of the source as estimated through SExtractor parameters (ISO_AREA, position angle).

⁸ Following Gehrels (1986), upper limits are estimated as $N + 1 + (N + 0.75)^{1/2}$, and lower limits as $N(1 - \frac{1}{9N} - \frac{1}{3\sqrt{N}})^3$.

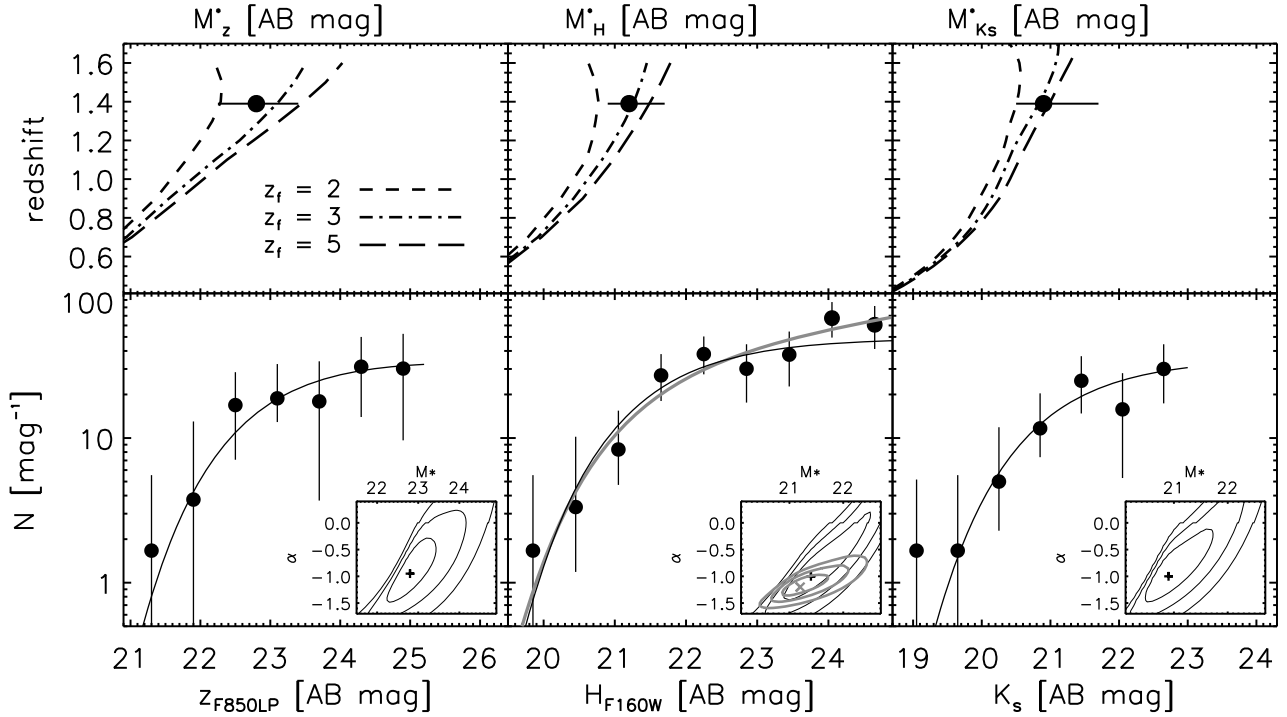


Fig. 3. *Bottom panels:* the luminosity function of galaxies in the central region (within ~ 700 kpc of the cluster center) of XMMU J2235, in the z , H and K_s bands. Solid symbols show binned counts (with 1σ errors, see text for details), and black lines show the best-fit Schechter function as determined for magnitudes brighter than $\sim M^* + 2$. Confidence levels (1, 2, 3σ) on the two relevant parameters (characteristic magnitude M^* and faint end slope α) are plotted in the small insets. In the central panel (H band LF) and corresponding inset, the gray lines show the best-fit Schechter function and confidence levels for the fit down to $\sim M^* + 4$. The formal best-fit values and 1σ errors for M^* and α , as fitted down to $\sim M^* + 2$, in the three passbands are: $M_z^* = 22.8 \pm 0.6$, $\alpha_z = -0.95 \pm 0.6$, $M_H^* = 21.4^{+1}_{-0.5}$, $\alpha_H = -1^{+1}_{-0.4}$ ($M_H^* = 21.2^{+0.5}_{-0.3}$, $\alpha_H = -1.2^{+0.2}_{-0.15}$ down to $\sim M^* + 4$), $M_{K_s}^* = 20.9^{+0.8}_{-0.4}$, $\alpha_{K_s} = -1.0^{+0.8}_{-0.5}$. *Upper panels:* the evolution of M^* with redshift as observed in the z , H and K_s band, according to Kodama & Arimoto (1997) models, for three formation redshifts $z_f = 2, 3, 5$. Solid symbols show M^* (and errors) as determined from the LFs in the lower panels.

LF determined for galaxies brighter than $M^* + 2$, as for the z and K_s bands, and down to $\sim M^* + 4$, which is only probed by the H band. In all cases, the best-fit faint-end slope is close to flat and the characteristic magnitude M^* is close to the predictions of passive evolution of the local M^* , assuming that the bulk of the stellar populations are formed at a redshift ~ 3 . This is shown in the upper panels of Fig. 3, showing the redshift evolution of M^* based on Kodama & Arimoto (1997) models, in each of the three passbands, together with the M^* determination from the LFs in the lower panels. The errors on M^* are determined based on the two-parameter confidence levels plotted in the small insets in the lower panels.

While the K_s band still samples the restframe near-infrared light, which can be considered as a probe of the stellar mass, the H and particularly z bands sample wavelengths more affected by recent or on-going star formation activity. Nonetheless, the LFs in all three passbands suggest a similar M^* evolution. The flat faint-end slope, and the measured M^* close to passive evolution predictions of the local cluster galaxy LF, point toward the LF bright end being similar to that of local clusters, beside evolution of the stellar populations. This extends to $z \sim 1.4$ previous findings on the early assembly of the massive galaxy populations in the cluster core regions (De Propriis et al. 1999; Nakata et al. 2001; Kodama & Bower 2003; Toft et al. 2003; Ellis & Jones 2004; Toft et al. 2004; Andreon 2006; Strazzullo et al. 2006; De Propriis et al. 2007; Muzzin et al. 2008; Mancone et al. 2010).

4. Stellar population properties of cluster galaxies

In the following, we investigate the properties of cluster galaxies in XMMU J2235, and of their host stellar populations, by means of direct, simpler approaches (as the color–magnitude diagrams) and of more detailed modeling (SED fitting with stellar population synthesis models), using the photometric and spectroscopic measurements described above.

4.1. Color–magnitude diagrams

Color–magnitude diagrams (CMDs) shown in the following refer to a region of about 3×3 arcmin² in the cluster center (the maximum distance from the BCG is about 1.2 Mpc). The H band image only covers a portion of this area, corresponding to a $\sim 2.4 \times 2.4$ arcmin² square centered on the BCG, which translates into $\sim 1200 \times 1200$ kpc² at $z = 1.39$.

Colors used in the following are based on resolution-matched magnitudes measured in a $1''$ aperture, which minimize the photometric errors (and possible contamination by neighbors), especially for fainter sources. We note that an independent, alternative approach based on model total magnitudes and aperture colors obtained via surface brightness fitting of each source, gives results in very good agreement with those obtained here (Nuñez et al., in prep.). We thus assume that the systematic errors affecting MAG_AUTO as an estimate of total magnitude, and aperture colors obtained as described above, do not significantly affect our results.

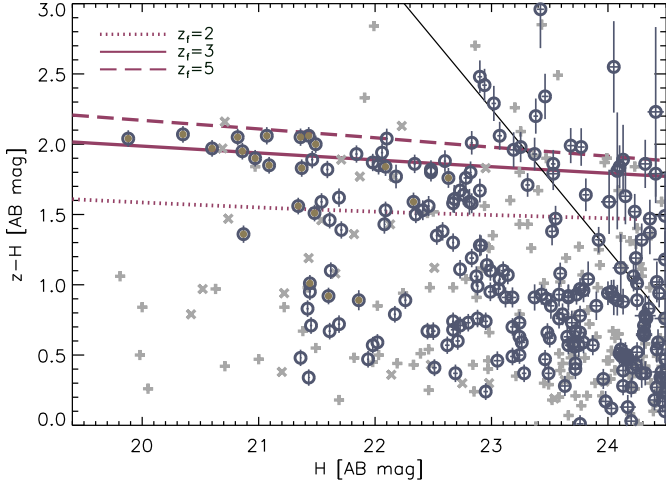


Fig. 4. The color–magnitude diagram in the central region ($r \leq 600$ kpc) of XMMU J2235. All sources in the field are shown, except for point–like sources. Filled circles are spectroscopic members and large empty circles show photo- z retained sources ($0.96 < z < 1.82$). Gray symbols (crosses and pluses) show spectroscopic and photo- z interlopers, respectively. The colored lines show the expected location of the red sequence at $z \sim 1.4$ based on Kodama & Arimoto (1997) models for different formation redshifts ($z_f = 2, 3, 5$, as indicated). The slanted continuous line shows the 10σ completeness (for the overall catalog, considering AUTO apertures). The plotted $z-H$ colors are derived from resolution-matched $1''$ aperture magnitudes, and error bars include the estimated error contribution from the resolution-matching procedure. Error bars are plotted only for retained sources.

In Fig. 4, we plot the $z-H$ vs. H CMD. All objects in the field are plotted, except for point-like sources which were removed (see Sect. 3). Spectroscopic cluster members are plotted as filled symbols, while spectroscopic interlopers are plotted as crosses. For consistency with Lidman et al. (2008) and Rosati et al. (2009), we define as cluster members all objects with $1.37 < z < 1.41$.

In addition to excluding spectroscopic interlopers, we can further clean the CMD in Fig. 4 of obvious foreground objects by excluding sources with a photo- z beyond 3σ of the cluster redshift (photo- $z < 0.96$ or > 1.82). These most likely interlopers are plotted in Fig. 4 as plus symbols, while the retained sources with photo- z within 3σ of the cluster redshift are plotted as empty circles. The whole $H < 24.5$ galaxy sample plotted in Fig. 4 contains 391 sources, out of which 205 have a photo- z within 3σ from the cluster redshift, 21 are spectroscopic cluster members, and 24 are spectroscopic interlopers. As explained above, the sample selected by retaining photo- z candidate members within 3σ of the cluster redshift is virtually 100% complete, but affected by a $\geq 50\%$ contamination, thus we point out that the only purpose of the “photo- z cleaned samples” plotted in the following Figs. 5 and 6 is to show more clearly the bright cluster population by removing the contamination of obvious foreground sources.

In Fig. 5, we plot the $z-H$ vs. H and $z-J$ vs. J CMDs, showing only spectroscopic cluster members and photo- z retained sources. The observed z band well matches the restframe U band of the cluster galaxies, and the J and H bands sample the restframe SED of cluster members at $\sim 5000 \text{ \AA}$ and $\sim 6700 \text{ \AA}$, respectively. The colors shown in Fig. 5 thus correspond approximately to restframe colors $U-B/U-V$ and $U-R$. While the observed $z-J$ color best samples the amplitude of the 4000 \AA break, the $z-H$ vs. H CMD benefits from the excellent photometric

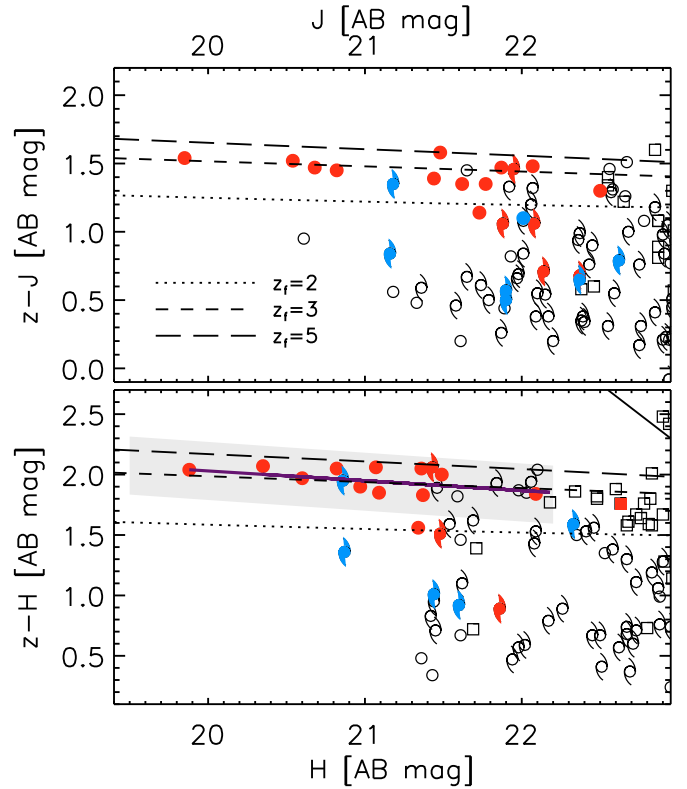


Fig. 5. Color–magnitude diagrams in the central region of XMMU J2235. Only spectroscopic members and photo- z retained sources ($0.96 < z < 1.82$) are shown. Filled blue and red symbols show spectroscopically confirmed members with and without detectable [OII] emission, respectively. The dotted, dashed and long-dashed lines show the expected location of the red sequence based on Kodama & Arimoto (1997) models for different formation redshifts. The dark purple line in the lower panel shows a fit to the red sequence galaxies within the gray shaded region. The shape of all symbols are coded according to morphological classification in the z band: circles are galaxies with $n_{\text{Sersic}} > 2$, spiral symbols are galaxies with $n_{\text{Sersic}} < 2$, squares are (mostly faint) objects for which no reliable classification is available.

accuracy and depth provided by HST imaging. Nonetheless, the presence of a tight red sequence is evident in both CMDs, with the zero-point and slope of the bright red sequence in good agreement with Kodama & Arimoto (1997) model predictions for a formation redshift $z_f \sim 3$. The intrinsic scatter of the bright $z-H$ red sequence (within the shaded area of Fig. 5) is estimated to be 0.08 ± 0.01 , independent of considering only morphological early-types or all red sequence galaxies. This estimate of the intrinsic scatter only takes into account photometric errors as estimated by SExtractor; considering the error introduced by the adopted PSF matching approach could lower the intrinsic scatter to values as low as 0.05 ± 0.015 .

We can roughly estimate the backward evolution of the XMMU J2235 red sequence bright-end (within the shaded area in Fig. 5) with a simplistic approach. The restframe $U-B$ scatter calculated from synthetic colors for the red-sequence galaxies is ~ 0.06 , in good agreement with previous estimates at similar redshifts (Blakeslee et al. 2006; Gobat et al. 2008; Mei et al. 2009). Assuming that the star formation histories of the bright red sequence galaxies may be described by a simple exponentially declining star formation rate with time-scale τ , we evolved the $z \sim 1.39$ red-sequence galaxies to earlier epochs (see also a more detailed analysis in Gobat et al. 2008). In general agreement

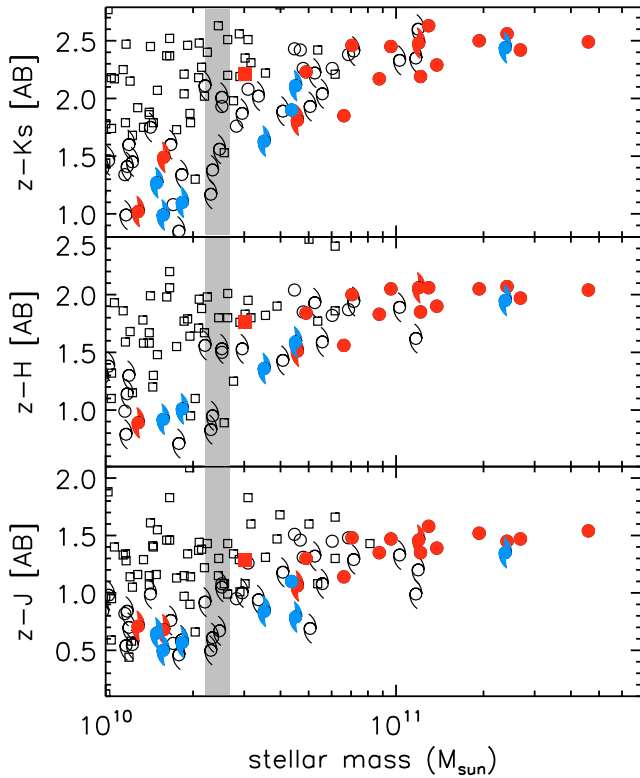


Fig. 6. Color-mass diagrams in the central region of XMMU J2235. Only spectroscopic members and photo- z retained sources ($0.96 < z < 1.82$) are shown. Symbols and color coding as in Fig. 5. The thick gray line across all panels shows the estimated mass completeness limit (see text).

with the Gobat et al. (2008) results based on the red sequence of RDCS1252 at $z \sim 1.2$, we find that beyond redshift 2 (e.g. ~ 1 Gyr earlier than the observed epoch for XMMU J2235) a significant part of the red sequence galaxies would no longer be classified as “red”, and the scatter of the remaining “red sequence” would be substantially larger than what measured in XMMU J2235. We note that this simplistic de-evolution of the red sequence does not take into account the whole population of massive galaxies in XMMU J2235 and the effects of dust extinction, thus does not include the contribution to the red sequence by reddened starbursts. By redshift ~ 2.3 , $\sim 40\%$ of the initial red-sequence sources would not be “red”; those still appearing as a “red sequence” would have an average age/ $\tau \sim 5$, thus they would have joined the red sequence relatively recently. This is in overall agreement with red-sequence observations at $z > 2$ in proto-clusters as well as in the field (e.g., Kodama et al. 2007; Kriek et al. 2008; Zirm et al. 2008).

We note that these CMDs are based on resolution-matched, fixed-aperture photometry in a $1''$ aperture, corresponding to a physical radius of ~ 4.2 kpc, and to about 1.8 times the median effective radius measured for the bright red-sequence early-types. Since the resolution-matching is performed independently on each passband image, the agreement of the formation epochs as estimated from the $z - H$ and $z - J$ CMDs suggests that the determined CMDs should not be significantly affected by systematics introduced by the resolution-matching procedure.

The presence of a tight red sequence in XMMU J2235 has already been reported in Lidman et al. (2008), based on the same high quality ground-based NIR photometry used in this work.

The Lidman et al. (2008) $J - K_s$ vs. K_s CMD was built within a distance of 900 kpc from the cluster center, and the parameters of the red sequence were determined based on 9 bright red-sequence galaxies within a smaller region ($r < 90$ kpc from the cluster center), four of which are spectroscopic members. Zero-point and slope of the $J - K_s$ vs. K_s red sequence are in good agreement with simple stellar population (SSP) models, reproducing the red sequence in the Coma cluster, formed at $z \sim 4$. Therefore, while the observed $J - K_s$ color at $z = 1.39$ is not the best choice to probe the stellar population ages, and while even high quality ground-based imaging hardly competes with HST imaging, especially in crowded fields, our $z - H$ vs. H color-magnitude relation substantially confirms the results of Lidman et al. (2008) on the presence of a tight red sequence of bright, passively evolving galaxies which formed their stars at high redshift. In addition, we note that the formation epoch of massive red sequence galaxies estimated in Fig. 5 by comparison with Kodama & Arimoto models, are in excellent agreement with the star-formation history derived by modeling the spectro-photometric data of these galaxies (Rosati et al. 2009) with Bruzual & Charlot (2003) models.

In Fig. 5, spectroscopic cluster members are color-coded according to the detection or non-detection of [OII] emission in their spectra; however, note that due to the quality of our spectra, [OII] equivalent widths of less than 5 \AA cannot be detected (Rosati et al. 2009). As noted in Lidman et al. (2008) and Rosati et al. (2009), emission line members tend to avoid the central area of the cluster, the closest emission-line member being at a distance of ~ 240 kpc from the BCG. We note that, even though the spectroscopic sample is generally not complete, according to the photo- z selection it is likely to be complete (in the central $\sim 1200 \times 1200 \text{ kpc}^2$ region) for sources brighter than M^* , and $\geq 80\%$ complete for masses larger than $10^{11} M_\odot$.

We also make use of the morphological information in the ACS z band to broadly classify sources in early and late morphological types. We are mainly interested in identifying late type galaxies on the red sequence, since these might be dusty star-forming galaxies landing on the red sequence because of dust reddening instead of the old age of their stars. As a result, these objects might bias our analysis and interpretation of the red sequence. The separation of early and late morphological types based on the Sersic index n_{Sersic} alone is known not to be very accurate (e.g., Blakeslee et al. 2003), and a multi-parametric classification should be adopted for a robust characterization. However, in this work we only aim at classifying galaxies in very broad morphological classes, which can be accomplished with good statistical accuracy by using the Sersic index alone (e.g. Blanton et al. 2003; Ravindranath et al. 2004; Pannella et al. 2006). In the following, we will use $n_{\text{Sersic}} > 2$ as the threshold to identify morphological early-types. With this selection, we are likely to include basically all ellipticals, and the vast majority of S0 galaxies, while having some contamination mainly from late-types with a significant bulge component. Such a threshold is a conservative choice from the point of view of the characterization of the red sequence sample, which will include some late morphological types. On the other hand, when considering the morphological mix of galaxy populations on the red sequence, we remind the reader that our early-type sample might be affected by such contamination.

In Fig. 5, we thus plot with different symbols galaxies for which we were able to perform a morphological analysis, according to their Sersic index (circles for $n_{\text{Sersic}} > 2$, spiral symbols for $n_{\text{Sersic}} < 2$). Most of the bright red-sequence galaxies in the cluster core are morphologically early types according to this

criterion ($\sim 90\%$ down to M^*). Visual inspection of the images of red sequence galaxies (gray shaded area in Fig. 5) confirmed the results based on the automated classification, in particular a dominance of early-type galaxies and a minor contribution from late types (often hosting a prominent bulge).

All but one of the spectroscopic members classified as morphological early types do not have detectable [OII] emission. The one exception is a galaxy with $n_{\text{Sersic}} \sim 2.4$ and intermediate colors ($z - J \sim 1.1$, $z - K_s \sim 1.8$), located more than 900 kpc away from the cluster center. [OII] emission is detected in most of the spectroscopic members classified as morphological late types. A fraction ($\sim 30\%$) of the (incomplete) sample of spectroscopic members classified as morphological late types lie on or close to the red sequence. Also, about 40% of the spectroscopic members morphologically classified as late-types within the studied field have no detectable [OII] emission, thus likely an [OII] $EW < 5 \text{ \AA}$. All but one of these late-type galaxies without detectable [OII] are relatively blue (as compared to the red sequence); none of them is located in the very central area of the cluster, the closest to the BCG is at a distance of about 150 kpc, while the others are more than 600 kpc away.

Unfortunately, our sample of late-type spectroscopic members is inevitably incomplete (many late-type candidate members are beyond the spectroscopic limit). Much larger samples will be needed to disentangle morphological and spectrophotometric evolution of cluster galaxies at this redshift. We also note that [OII] emission might also be due to AGN activity rather than star formation (Yan et al. 2006), especially for objects with a typically red SED. Nonetheless, we also note that the only [OII] emitter actually lying on the red sequence has a late-type morphology; its colors would be $\sim 0.2\text{--}0.3$ mag bluer in a larger aperture including the extended disk. This source is located at a distance of ~ 860 kpc from the cluster center. None of the red-sequence galaxies shown in Fig. 5 is detected as an X-ray point source. We note that the 190 ks Chandra observations of this field allow the detection of AGN with X-ray luminosities $L_X \gtrsim 10^{43} \text{ erg s}^{-1}$ in the 2–10 keV band.

4.2. Color-mass diagrams and star formation rates

We show in Fig. 6 the color-stellar mass diagram in the central cluster area, as in Fig. 5. While overall similar to the color–magnitude diagram in terms of bimodality of the galaxy populations, the color-mass diagram yields more fundamental insight because of the disentanglement between color, magnitude, and mass-to-light ratio.

Colors were derived from resolution-matched photometry measured in $1''$ apertures, as described above. The derivation of stellar masses is described in Sect. 2.3, and an approximate estimate of the mass completeness limit of this sample, derived from the z band 10σ completeness assuming a SSP of solar metallicity formed at $5 < z < 10$, is shown by the thick gray line in Fig. 6.

Figure 6 confirms that high mass galaxies ($\gtrsim 10^{11} M_\odot$) are already in place in the core region of XMMU J2235, and that this high-mass population is dominated by red-sequence galaxies, mainly of early-type morphology, generally lacking evidence of significant star formation activity. The stellar mass of the BCG is close to the stellar mass of local BCGs in massive clusters (see Collins et al. 2009; Stott et al. 2010, for a broader picture). According to semi-analytical predictions (De Lucia et al. 2006), a BCG at $z \sim 1.4$ will have typically assembled only $\sim 20\%$ of the final stellar mass it will reach at $z = 0$. In such a model, the BCG of XMMU J2235 would thus eventually become an object

of $2.3 \times 10^{12} M_\odot$; while not impossible, this would certainly put it at the very high-mass end of local BCGs. We note however that this same model predicts a slower evolution for BCGs of most massive, X-ray luminous clusters as XMMU J2235.

Figure 6 clearly shows that, even at $z \sim 1.4$, there are essentially no blue galaxies in the most massive populations living in the core of such a massive cluster. As expected, going to lower masses the importance of late-type galaxies (from both the morphological and the photometric point of view) increases. It may be interesting to note that blue, disk-dominated spectroscopic members with [OII] emission generally lie at masses below $\sim 5 \times 10^{10} M_\odot$. We note again here that the spectroscopic sample is biased against red galaxies at these masses, because of their intrinsic faintness due to their higher mass-to-light ratio, and to the lack of emission lines.

While keeping in mind that the rest-frame FUV light may be heavily affected by dust attenuation, we further note here that the rest-frame 1500 \AA flux of massive ($> 6 \times 10^{10} M_\odot$) red sequence early-types is indeed consistent with these galaxies hosting no significant star formation. After removing galaxies whose U band photometry is likely contaminated by other sources, we stacked U band images for eight early-types more massive than $6 \times 10^{10} M_\odot$ (six out of these eight are spectroscopic members). We found no significant detection and obtained a 5σ U -band upper limit of 27.5 AB mag, corresponding to a (not dust-corrected) star formation rate (SFR) of $\sim 0.15 M_\odot \text{ yr}^{-1}$ (for comparison, Rettura et al. 2010 estimated by U -band stacking an upper limit of $\sim 0.3 M_\odot \text{ yr}^{-1}$ for the SFR in massive early-types in the $z \sim 1.2$ cluster RDCS J1252-2927).

For comparison, the SFR of the spectroscopic members lying below the $z_f = 2$ model in Fig. 5 was also estimated based on the measured U band (rest-frame $\sim 1500 \text{ \AA}$) photometry. Since we know that these are star-forming sources, we estimated a dust attenuation correction for the $\sim 1500 \text{ \AA}$ rest-frame luminosity from the restframe far-UV – near-UV color (Daddi et al. 2007; Salim et al. 2007; Pannella et al. 2009a), which in our case is sampled by the observed U and R bands. SFRs derived with these dust attenuations following e.g. Daddi et al. (2007), range between 6 and 50–90 $M_\odot \text{ yr}^{-1}$ depending on the assumed relation, with a median of $\sim 20 M_\odot \text{ yr}^{-1}$. Specific SFRs (SSFR, SFR/stellar mass) are between 0.2 and 2–6 Gyr^{-1} (also depending on the specific relation used), with an average of $\sim 1 \text{ Gyr}^{-1}$. We remind the reader of the uncertainties which affect these values due to the scatter in the assumed relations, filter mis-match, and general difficulties in estimating correct dust attenuation values for a given source/sample (for instance, Salim et al. 2007 note that their attenuations as a function of UV color are systematically lower than other estimates by e.g. Meurer et al. 1999; Seibert et al. 2005). For comparison we also estimated dust extinction for these sources with a different approach, based on the correlation between dust attenuation and stellar mass for star-forming galaxies, assuming that these objects follow a correlation similar to that of field galaxies at comparable redshift. We estimated the dust attenuation for the 1500 \AA rest-frame luminosity based on the galaxy stellar mass according to the relation determined for $z \sim 1.7$ galaxies in Pannella et al. (2009a), obtaining an independent estimate of the SFR. We note that since the relation between stellar mass and dust attenuation is redshift dependent (given the secular decline of (S)SFR), we corrected for the cosmic time difference between $z = 1.7$ and $z = 1.39$ according to Eq. (2) in Pannella et al. (2009a). The SFRs for the blue cluster members derived in this way range between $\sim 6 M_\odot \text{ yr}^{-1}$ and $\sim 100 M_\odot \text{ yr}^{-1}$, with a median of $\sim 25 M_\odot \text{ yr}^{-1}$.

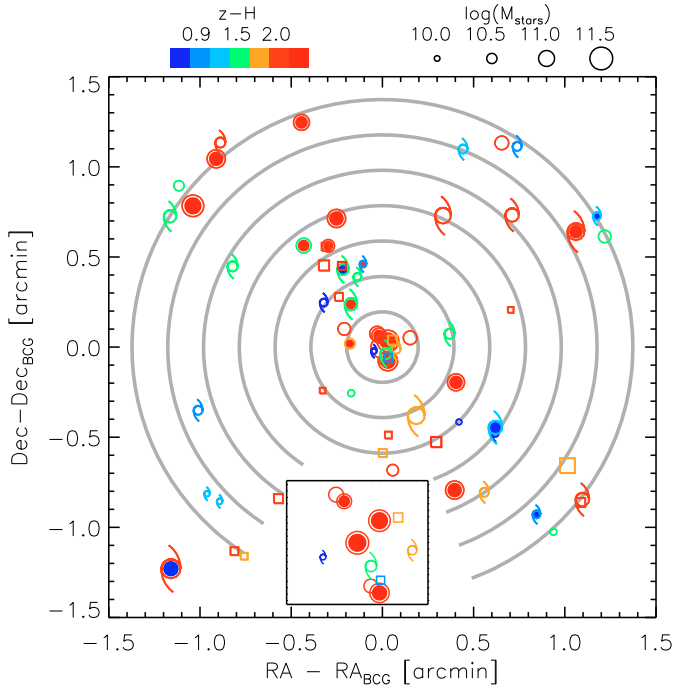


Fig. 7. The projected distribution around the cluster BCG of 2σ retained photo- z candidate members (spectroscopic interlopers are not plotted). Symbol shape is coded as in Figs. 5 and 6, external color coding reflects the $z-H$ color while symbol size scales with stellar mass (as indicated). Color filling, for spectroscopic members, is blue for galaxies with detected [OIII] emission, red otherwise. The small inset at the bottom of the plot shows a larger view of the central $\sim 0.2 \times 0.2$ arcmin² ($\sim 98 \times 98$ kpc²). Gray lines show radii of 100 to 700 kpc (with a step of 100 kpc).

SSFRs range between ~ 0.3 Gyr⁻¹ and ~ 3 Gyr⁻¹, with an average $SSFR \sim 1.3$ Gyr⁻¹. Stellar masses of these sources are in the range $1-7 \times 10^{10} M_{\odot}$. Due to the observational bias, most of the passive spectroscopic members lie at masses above this range. At masses below $\sim 5 \times 10^{10} M_{\odot}$, with the available spectroscopic data, redshifts can be measured only for sources with a relevant amount of star formation (and without extreme dust extinction). As Fig. 6 shows, the star forming spectroscopic members discussed above are among the bluest sources in the cluster galaxy populations in their mass range.

Finally, Fig. 7 summarizes the information concerning stellar masses, (spectro-)photometric and morphological properties of 2σ photo- z retained candidate cluster members together with their projected distance from the cluster centre. Recent work on high redshift clusters at $z \sim 1.45$ and 1.62 , corresponding to cosmic times about 0.2 Gyr and 0.6 Gyr earlier than XMMU J2235, suggested that a significant star formation activity might be occurring in the very central regions ($r < 250-500$ kpc, Hilton et al. 2010; Tran et al. 2010) of clusters in a less advanced evolutionary stage. However, as Fig. 7 shows, star formation appears to be effectively quenched in the core of a more evolved, massive X-ray luminous cluster as XMMU J2235. The relevance of very reddened star formation contaminating the cluster red sequence could be addressed with future observations (NIR spectroscopy, Herschel IR photometry), however, even though the rest-frame NUV (U band) photometry might be affected by dust extinction, the early-type morphological appearance and spectral features of the central massive red galaxies suggest that these are more likely passive early-types than highly attenuated starbursts.

5. Stellar masses and sizes of massive cluster early-types

The above analysis in the central regions of a particularly massive, distant X-ray luminous cluster shows that the high-mass population of cluster galaxies primarily of early-type morphology is substantially in place at epochs earlier than redshift one, in relation to both the formation of the bulk of their stars (at $z > 2$) and of the assembly of the bulk of their stellar mass. This points toward little evolution occurring in massive galaxy populations in the most dense environments over the last 9 billion years. On the other hand, it is interesting to remember that the structural properties of such massive objects might be different from those of similar galaxies in the local Universe. As pointed out in several studies (e.g., Daddi et al. 2005; Trujillo et al. 2006b,a, 2007; Longhetti et al. 2007; Cimatti et al. 2008; Buitrago et al. 2008; van der Wel et al. 2008; Damjanov et al. 2009; Rettura et al. 2010; Williams et al. 2010; Taylor et al. 2010, and references therein), massive early-type galaxies at high redshift appear to be (on average) more compact than their local counterparts, their size being smaller than that of local early-types of comparable mass (but see also results and discussion in e.g. Mancini et al. 2010; Onodera et al. 2010; Valentinuzzi et al. 2010; Saracco et al. 2010, and references therein). Indeed, as shown in Fig. 8, also the massive early-type galaxies in the core of XMMU J2235 appear to be generally smaller than those in the local Universe.

Figure 8 shows the stellar mass against the (circularized) effective radius⁹ as measured from the surface brightness fit in the z band (Sect. 2.4), for bright early-type¹⁰ red sequence galaxies (within the gray shaded area in Fig. 5). Most of this sample is made of spectroscopic cluster members. For comparison we show the local stellar mass vs. size relation as measured for SDSS early-type galaxies by Shen et al. (2003), which is commonly used as the local reference. We note that the size used by Shen et al. (2003) was measured in the z band, while in our case galaxy sizes are measured in the observed z band, corresponding to the restframe U band, which might imply issues due to morphological K -corrections. However, sizes measured in bluer bands are expected to be larger than sizes measured in redder bands (e.g., Barden et al. 2005; McIntosh et al. 2005; Trujillo et al. 2007). Therefore our galaxy sizes, if measured in the restframe z band would be, if anything, smaller than those plotted in Fig. 8, as it is indeed suggested for this very sample by the comparison of surface brightness fitting results in the observed z and K_s passbands (Nuñez et al., in prep.). Therefore, taken at face value, the comparison of our early-type sample with the local Shen et al. (2003) reference implies that the size of massive early-types in XMMU J2235 is on average about $\sim 50\%$ of what expected based on the local relation (median $r/r_{z=0} = 0.46 \pm 0.08$). We note that the most massive object in Fig. 8 is the cluster BCG; while the size of this galaxy is quite large and it lies on the local relation, we note that BCGs tend

⁹ Six (one) sources out of the 15 plotted in Fig. 8 have a formal uncertainty on their size lower than 15% (10%). Keeping into account results from simulations or multiple independent fitting (e.g. Pignatelli et al. 2006; Buitrago et al. 2008; Pannella et al. 2009b) on the typical uncertainty on the galaxy size ($\sim 10-15\%$) achievable by surface brightness fitting for sources of S/N similar to those used here, we increase the error bar for these six sources to reflect an uncertainty of 15%.

¹⁰ Galaxies in this sample were classified as “early-types” based on their Sérsic index larger than 2, as discussed above. We note that out of 15 galaxies plotted in Fig. 8, only two (with Sérsic indices 2.3 and 2.4) would not have entered the “early-type sample” if using a Sérsic index threshold of 2.5.

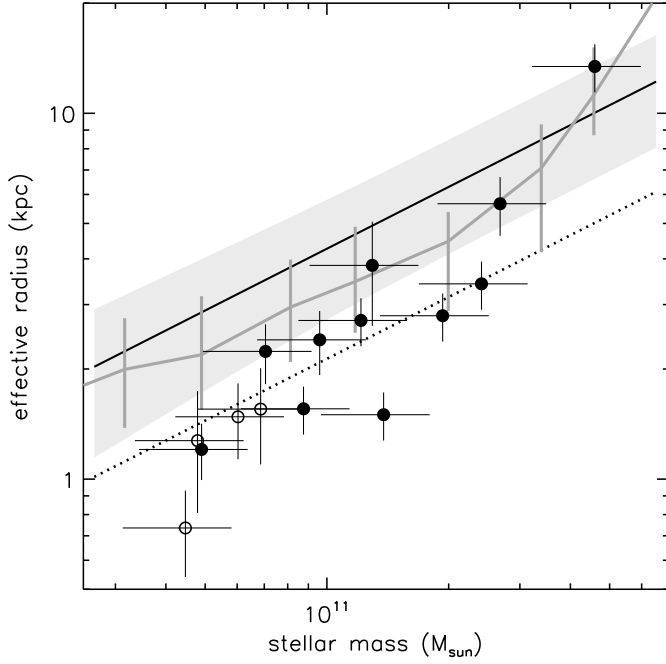


Fig. 8. The stellar mass vs. size relation for massive red-sequence early-type galaxies in the core of XMMU J2235. Filled symbols are spectroscopic members, empty symbols are sources with photo- z within 3σ of the cluster redshift. The black line and shaded area show the Shen et al. (2003) determination of the local stellar mass vs. size relation and its scatter (1σ), based on a sample of SDSS early-types. The dotted line shows the Shen et al. (2003) relation shifted by a factor 2 in size. The gray line with errorbars shows the local mass vs. size relation determined by Valentinuzzi et al. (2010) for a sample of nearby cluster galaxies.

to be larger than similarly massive (non-BCG) galaxies (e.g., von der Linden et al. 2007).

The smaller sizes of XMMU J2235 massive early-types compared to local early-types suggest a scenario where the evolution of these massive red-sequence galaxies is not actually fully completed at early epochs, as would be suggested by the color–magnitude and color-mass relations, as well as the LF evolution. This leaves room for processes such as minor (and likely fairly dry) merging events to be relevant at later epochs to shape the final structural properties of these galaxies, without substantially altering their stellar masses and stellar populations (see e.g. Hopkins et al. 2010, and references therein; see also discussion in Nipoti et al. 2009).

On the other hand, we should note that the comparison of the stellar mass vs. size relation with a local sample, as shown in Fig. 8, may be affected by systematics in the determination of stellar masses at different redshifts, observational biases in the determination of galaxy sizes (Pannella et al. 2009b; Mancini et al. 2010), and a possible mismatch between the observed high redshift sample and the local reference, which are discussed in more detail below.

In Fig. 8 we also plot the local stellar mass vs. size relation for a sample of nearby cluster galaxies as measured by Valentinuzzi et al. (2010). While consistent at 1σ with the Shen et al. (2003) relation, the Valentinuzzi et al. (2010) determination is systematically offset (possibly due to an offset with respect to the stellar mass estimates used in Shen et al. 2003, rather than because of environmental effects, see discussion in the original paper – see also results from Graham & Worley 2008). Using the

Valentinuzzi et al. (2010) relation as the local reference thus reduces the difference between our sample and local massive (cluster) early-types (median $r/r_{z=0} = 0.64 \pm 0.08$).

In addition, Maraston (2005) has pointed out how a different treatment of the thermally pulsing asymptotic giant branch (TP-AGB) phase of stellar evolution may introduce additional (to those mentioned in Sect. 4.2) systematics in the stellar masses, whose significance depends on the age of the stellar populations. This may be particularly relevant when comparing early-type galaxies at different redshifts, because while local early-types are too old for TP-AGB phase making a significant difference, at higher redshifts they inevitably become closer to hosting the intermediate age stellar populations for which a different TP-AGB phase treatment may have an important effect. For the sample relevant to Fig. 8, stellar masses estimated with the Maraston (2005) models are lower by about 0.1 dex than the masses plotted, estimated with Bruzual & Charlot (2003). Using these lower masses, the size of galaxies in Fig. 8 are $\sim 50\%$ and $\sim 70\%$ of those of early-types at $z = 0$, based on the local relations by Shen et al. (2003) and Valentinuzzi et al. (2010) ($r/r_{z=0} = 0.5 \pm 0.1$ and 0.72 ± 0.1 , respectively). We note that if we use the updated version of the Bruzual & Charlot (2003) models (often referred to as CB07), incorporating an improved prescription for the treatment of the TP-AGB phase, stellar masses for the Fig. 8 sample are lower (in median) by 0.03 dex; CB07 mass estimates for this sample range from almost 30% lower to $\sim 10\%$ higher compared to Bruzual & Charlot (2003).

A combination of systematics in stellar masses and mismatch with the local reference relation might thus shift the (median) difference in size of XMMU J2235 and local early-types between a factor slightly over 2 and a factor 1.4.

We note that other effects might also systematically bias the stellar masses and sizes used above. Again, we recall that our sizes were estimated in the restframe U band, while we are comparing with local galaxy sizes measured in the z (Shen et al. 2003) and V (Valentinuzzi et al. 2010) passbands. Based on previous work (McIntosh et al. 2005; Barden et al. 2005; Trujillo et al. 2007; Szomoru et al. 2010), correcting our sizes to the restframe z/V bands might reduce our sizes by a factor of up to 30%, and thus increase the median difference in size with local counterparts to up to a factor ~ 3 (using Bruzual & Charlot 2003 stellar masses, and the Shen et al. 2003 local reference).

We also remind the reader that the stellar masses used here were derived assuming a fixed, solar metallicity. Should the metallicity of the galaxies in Fig. 8 be lower than solar, their stellar masses would be higher, by a factor about 15% and 2% for metallicities of 0.004 and 0.008, respectively. If their metallicity is supersolar, their stellar masses would be lower, by a factor $\sim 30\%$ for a metallicity of 0.05.

Finally, we note that the sizes we used were estimated based on a Sersic profile fit with varying n_{Sersic} . Therefore, for the sample of early types plotted in Fig. 8, n_{Sersic} is not fixed to 4, but ranges between ~ 2.5 –6 with an average $n_{\text{Sersic}} \sim 3.5$. Because of the correlation between the estimated n_{Sersic} and size, an object with a $n_{\text{Sersic}} = 4$ profile which is fitted with a lower Sersic index (possibly due to the faintness of the source) will also have its size biased to a lower value. In order to estimate the relevance of such an effect, we fitted all sources in Fig. 8 with n_{Sersic} fixed to 4. This produces a very mild difference (on average $\lesssim 15\%$) in the estimated sizes, and overall negligible difference ($\lesssim 5\%$) in the evolution factors quoted above.

Although the above results imply an evolution of the stellar mass vs. size relation by a factor of about 1.4 to more than 2, this evolution does not necessarily imply that the individual galaxies in

our early-type sample will evolve by this factor by redshift zero. Several studies showed how the population of early-type galaxies is increased, as a function of cosmic time, by the evolution of late-type, star-forming galaxies into quiescent early-types (e.g., among many others, [Bell et al. 2004](#); [Pannella et al. 2006](#); [Faber et al. 2007](#); [Brown et al. 2007](#); [Franx et al. 2008](#), and references therein). It is thus very likely that a significant fraction of early-types at $z = 0$ were still forming stars at $z = 1.4$ (or did not yet have an early-type morphology), and were added to the local “reference” early-type sample at later cosmic times. Together with the present-day correlation (at fixed mass) between galaxy size and age of its host stellar populations, this may indeed suggest that the comparison of high-redshift early-type samples with local samples might artificially produce a “size evolution” signature, because the high-redshift sample does not account for the whole progenitor population of the local sample (see discussion in e.g. [Franx et al. \(2008\)](#); [van der Wel et al. \(2009\)](#); [Valentinuzzi et al. \(2010\)](#); [Bernardi et al. \(2010\)](#); [Williams et al. \(2010\)](#)). According to [van der Wel et al. \(2009, their Fig. 5\)](#) and [Valentinuzzi et al. \(2010, their Fig. 4\)](#), the systematic exclusion from the high-redshift sample of the progenitors of younger local early-types, which tend to have larger sizes, might produce a difference in size of a factor as large as 1.3 at the redshift of XMMU J2235.

A definite conclusion on the actual relevance of size evolution for our sample of massive cluster early-types is thus precluded by the possible biases mentioned above. It remains clear that the significant range of galaxy sizes at all redshifts requires much larger samples in order to draw a conclusive picture of the mass and environmental dependence of galaxy size evolution.

Finally, for the sake of completeness, we note that by comparing the sizes of our spectroscopic members of *late-type* morphology with the typical size of late-type galaxies in the nearby Universe ([Shen et al. 2003](#); as well as [Maltby et al. 2010](#) specifically in “cluster” and “cluster core” environments), we cannot find evidence of significant size evolution at fixed stellar mass for disk-dominated galaxies. The formal difference we find by comparing our late-type sizes at masses $10^{10} - 10^{11} M_{\odot}$ with cluster galaxies at $z \sim 0.2$ ([Maltby et al. 2010](#)) would be up to $\sim 15\%$ (for our standard [Bruzual & Charlot 2003](#) stellar masses), but given the large uncertainties inherent in the comparison (as discussed above), and the fact that our spectroscopic late-type sample suitable for this comparison is small (≤ 10 galaxies) and incomplete, we cannot derive any definite conclusion.

6. The stellar mass function

Since the observed K_s -band light probes the rest-frame z band of galaxies at the cluster redshift, the K_s -band LF derived in Sect. 3 can be used to estimate the stellar mass function of galaxies in the central region ($r \lesssim r_{500}$) of XMMU J2235.

We note that, while a galaxy NIR luminosity has a milder sensitivity to recent star formation and dust attenuation as compared to luminosity at shorter wavelengths, stellar masses derived from the NIR luminosity alone may still suffer from systematics of up to a factor ~ 2 depending on different mass-to-light (M/L) ratios of different galaxies. Based on stellar masses of sources with photo- z s within 2σ of the cluster redshift, we calibrated the stellar mass vs. observed K_s -band luminosity relation finding a scatter of ~ 0.3 dex for the whole sample and of ~ 0.15 dex when considering blue and red galaxies separately (using a color threshold of $z - H \simeq 1.5$).

We therefore applied a statistical correction for different M/L ratios of cluster galaxies in the K_s -band selected sample,

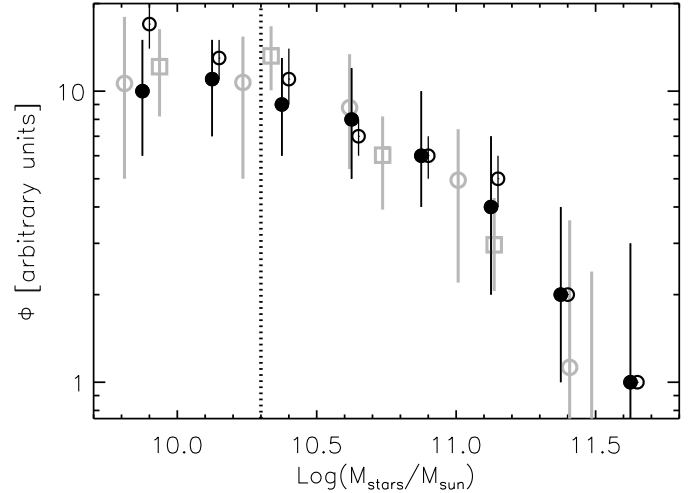


Fig. 9. The galaxy stellar mass function in the central region of XMMU J2235, as derived from the K_s -band LF (solid symbols). Empty black circles show the stellar mass function derived from individual SED-estimated stellar masses of spectroscopic and photo- z retained members (see text for details). Gray symbols show previous determinations ([Kodama & Bower 2003](#); [Strazzullo et al. 2006](#)) at $z \sim 1$ (squares) and $z \sim 1.2$ (circles). All mass functions are arbitrarily rescaled. The dotted line shows the mass completeness limit as estimated from the K_s image 10σ completeness.

and derived the mass function and its uncertainties as follows. Firstly, we estimated the fraction of red and blue cluster galaxies as a function of K_s -band luminosity based on the 2σ photo- z retained sample, based on both the $z - H$ and $z - J$ colors, yielding consistent results. Because of the $\sim 100\%$ completeness and $\sim 50\%$ contamination of this sample, we may expect that the estimated relative contributions of red and blue cluster galaxies are possibly biased toward a higher blue fraction, since the interlopers contaminating our sample will be, on average, preferentially bluer than cluster galaxies. This would result in a possibly lower M/L ratio used to statistically convert the K_s -band light to stellar mass (and thus lower masses).

Once the relative contributions of red and blue galaxies, and the typical M/L ratios of these two populations were determined, the K -band LF was translated into a stellar mass function by means of 1000 realizations taking into account the error on the LF (as plotted in Fig. 3), the estimated scatter in the M/L ratios of red and blue galaxies, and the error in the red/blue galaxy fractions.

The derived stellar mass function is shown in Fig. 9. Solid black symbols and errorbars show the median and 16–84th percentiles of the distribution obtained through the 1000 realizations. For comparison, we also show (empty black symbols) the stellar mass function that is directly obtained from the individual SED-estimated stellar masses of the spectroscopic members plus photo- z retained sources randomly sampled assuming a $\sim 50\%$ contamination by interlopers. These two largely independent determinations of the stellar mass function in the central region of XMMU J2235 are perfectly consistent. The shape of the mass function determined here is in very good agreement with (arbitrarily rescaled) previous measurements in clusters at $z \sim 1$ and $z \sim 1.2$ ([Kodama & Bower 2003](#); [Strazzullo et al. 2006](#), both scaled to a Kroupa IMF), once again suggesting an early assembly of massive galaxies at least in overdense environments, with the high-mass end population essentially in place at one third of the Hubble time.

The area considered here lies within $r < 90'' = 765$ kpc, which is very close to the estimated r_{500} for XMMU J2235 ($r_{500} \sim 0.75$ Mpc, Rosati et al. 2009). The total projected stellar mass within this area, inferred from integrating the K_s band LF and converting the total K -band luminosity ($L_{K,500,proj} = \Phi^* L^* \Gamma(2+\alpha) = 11 \pm 2 \times 10^{12} L_\odot$) to stellar mass, is $M_{stars,500,proj} = 6_{-3}^{+6} \times 10^{12} M_\odot$, with errors including the uncertainties on the LF parameters and the scatter in the galaxy M/L ratios. For comparison, the stellar mass in galaxies more massive than $\sim 10^{10} M_\odot$, statistically determined from the photo- z retained sample within the same area (see mass function in Fig. 9), is $\sim 3 \times 10^{12} M_\odot$.

Following Rosati et al. (2009) the total projected mass within this radius is $M_{tot,500,proj} = 7 \pm 2 \times 10^{14} M_\odot$. The ratio of total mass to K -band luminosity in the projected area within r_{500} is thus $M_{tot,500,proj}/L_{K,500,proj} = 60 \pm 20 M_\odot/L_\odot$, while the stellar mass fraction is $M_{stars,500,proj}/M_{tot,500,proj} = 0.009_{-0.007}^{+0.01}$, in close agreement with determinations for massive clusters at lower redshifts (e.g., Lin et al. 2003; Etori et al. 2009; Giodini et al. 2009; Andreon 2010).

7. Summary

We presented a study of galaxy populations in the core of the massive cluster XMMU J2235 at $z = 1.39$, making use of high quality VLT and HST multi-wavelength photometry in seven passbands from U to K_s , sampling the rest-frame SED of cluster members from the NUV to the NIR.

We derived luminosity functions in the z , H , and K_s bands, approximately corresponding to the rest-frame U , R , and z bands. These extend the study of the galaxy luminosity function in massive X-ray luminous clusters beyond $z \sim 1.3$, and are among the deepest determinations at $z > 1$. All three determinations of the luminosity function, probing down to $\sim M^* + 2$ or $M^* + 4$ depending on the passband, are consistent with having a flat faint-end slope and a characteristic magnitude M^* close to passive evolution predictions of the M^* of local massive clusters with a formation redshift $z > 2$.

The color-magnitude and color-mass diagrams in the core region of XMMU J2235 show evidence of a tight (intrinsic scatter $\lesssim 0.08$) red sequence of massive galaxies, with overall old stellar populations ($z_f > 2$), no evidence of significant on-going star formation ($SFR < 0.2 M_\odot \text{ yr}^{-1}$), and generally early-type morphology. The spectroscopic sample is essentially complete at the high-mass end, and strongly suggests that the most massive cluster galaxy populations in the core of this cluster are already dominated by early-type galaxies, both in terms of galaxy structure and of overall spectro-photometric properties.

Star formation appears effectively quenched at masses higher than $\sim 6 \times 10^{10} M_\odot$. Also, active star formation is suppressed in the very central regions, with all spectroscopically confirmed star forming cluster members located at $r \gtrsim 250$ kpc from the BCG.

In agreement with previous work at lower redshifts, these data point toward an early assembly of massive cluster galaxies, not only in terms of the formation of their stars, as suggested by their broad-band SEDs, as well as by their spectra (Rosati et al. 2009), but also of the assembly of their stellar mass, as suggested by the SED-derived stellar masses of individual sources, by the close-to-passive evolution of the luminosity function bright-end, and by the galaxy stellar mass function. As an additional evidence that XMMU J2235 is in a very advanced evolutionary stage already at this redshift, we estimate a stellar mass fraction within r_{500} of about 1%, similar to local massive clusters.

On the other hand, comparing the size of the massive red-sequence galaxies to the size of similarly massive local early-types, suggests a possible size evolution of up to a factor ~ 2 . This may imply that, in spite of the overall early assembly of these sources, room is left for processes like minor (and likely dry) merging to shape the structural properties of these objects to resemble those of their local counterparts, without substantially affecting their stellar mass or galaxy populations. We discussed how the role of possible systematics makes it still difficult to draw firm conclusions on the magnitude of such a size evolution, and on whether this evolution might be different from the one estimated in field galaxy samples over the same redshift range. Much larger samples of high-redshift (cluster) early-type galaxies are needed to derive a conclusive picture of the mass and environmental dependence of their size evolution.

Future observations at IR, mm and radio wavelengths, probing dust-unbiased star formation and the cold gas component, will enhance our understanding of the mass growth, star formation, and structural evolution of high-redshift cluster galaxies.

Acknowledgements. We are grateful to T. Kodama for providing us with results from his elliptical galaxy evolution models. We thank the anonymous referee for a constructive report which helped us to improve the presentation of this work. V.S. acknowledges support under the ESO visitor program in Garching during the completion of this work. V.S. and M.P. acknowledge support from the Max-Planck Society and the Alexander von Humboldt Foundation, and from NASA through Jet Propulsion Laboratory contract No.1289215. The National Radio Astronomy Observatory is a facility of the National Science Foundation operated under cooperative agreement by Associated Universities, Inc. P.R. acknowledges support by the DFG cluster of excellence Origin and Structure of the Universe. Financial support for this work was partly provided by NASA through program GO-10496 from the Space Telescope Science Institute, which is operated by AURA, Inc., under NASA contract NAS 5-26555. This work was also supported in part by the Director, Office of Science, Office of High Energy and Nuclear Physics, of the US Department of Energy under Contract No. AC02-05CH11231.

References

- Andreon, S. 2006, A&A, 448, 447
 Andreon, S. 2008, MNRAS, 386, 1045
 Andreon, S. 2010, MNRAS, 407, 263
 Andreon, S., Punzi, G., & Grado, A. 2005, MNRAS, 360, 727
 Andreon, S., Maughan, B., Trinchieri, G., & Kurk, J. 2009, A&A, 507, 147
 Barden, M., Rix, H., Somerville, R. S., et al. 2005, ApJ, 635, 959
 Bell, E. F., Wolf, C., Meisenheimer, K., et al. 2004, ApJ, 608, 752
 Bender, R., Appenzeller, I., Böhm, A., et al. 2001, in Deep Fields, ESO astrophysics symposia proceedings (Springer-Verlag), ed. S. Cristiani, A. Renzini, & R. E. Williams, 96
 Bernardi, M., Shankar, F., Hyde, J. B., et al. 2010, MNRAS, 404, 2087
 Bertin, E., & Arnouts, S. 1996, A&AS, 117, 393
 Blakeslee, J. P., Franx, M., Postman, M., et al. 2003, ApJ, 596, L143
 Blakeslee, J. P., Holden, B. P., Franx, M., et al. 2006, ApJ, 644, 30
 Blanton, M. R., Hogg, D. W., Bahcall, N. A., et al. 2003, ApJ, 594, 186
 Bower, R. G., Benson, A. J., Malbon, R., et al. 2006, MNRAS, 370, 645
 Brimiouille, F., Lerchster, M., Seitz, S., Bender, R., & Snigula, J. 2008 [arXiv:0811.3211]
 Brown, M. J. I., Dey, A., Jannuzi, B. T., et al. 2007, ApJ, 654, 858
 Bruzual, G., & Charlot, S. 2003, MNRAS, 344, 1000
 Buitrago, F., Trujillo, I., Conselice, C. J., et al. 2008, ApJ, 687, L61
 Cimatti, A., Cassata, P., Pozzetti, L., et al. 2008, A&A, 482, 21
 Coleman, G. D., Wu, C.-C., & Weedman, D. W. 1980, ApJS, 43, 393
 Collins, C. A., Stott, J. P., Hilton, M., et al. 2009, Nature, 458, 603
 Daddi, E., Renzini, A., Pirzkal, N., et al. 2005, ApJ, 626, 680
 Daddi, E., Dickinson, M., Morrison, G., et al. 2007, ApJ, 670, 156
 Damjanov, I., McCarthy, P. J., Abraham, R. G., et al. 2009, ApJ, 695, 101
 Dawson, K. S., Aldering, G., Amanullah, R., et al. 2009, AJ, 138, 1271
 De Lucia, G., Springel, V., White, S. D. M., Croton, D., & Kauffmann, G. 2006, MNRAS, 366, 499
 De Lucia, G., Poggianti, B. M., Aragón-Salamanca, A., et al. 2007, MNRAS, 374, 809
 De Propris, R., Stanford, S. A., Eisenhardt, P. R., Dickinson, M., & Elston, R. 1999, AJ, 118, 719

- De Propriis, R., Stanford, S. A., Eisenhardt, P. R., Holden, B. P., & Rosati, P. 2007, *AJ*, 133, 2209
- Demarco, R., Wilson, G., Muzzin, A., et al. 2010, *ApJ*, 711, 1185
- Eisenhardt, P. R., Stern, D., Brodwin, M., et al. 2004, *ApJS*, 154, 48
- Eisenhardt, P. R. M., Brodwin, M., Gonzalez, A. H., et al. 2008, *ApJ*, 684, 905
- Ellis, S. C., & Jones, L. R. 2004, *MNRAS*, 348, 165
- Ettori, S., Morandi, A., Tozzi, P., et al. 2009, *A&A*, 501, 61
- Faber, S. M., Willmer, C. N. A., Wolf, C., et al. 2007, *ApJ*, 665, 265
- Fassbender, R. 2008, Ph.D. Thesis [arXiv:0806.0861]
- Franx, M., van Dokkum, P. G., Schreiber, N. M. F., et al. 2008, *ApJ*, 688, 770
- Gabasch, A., Bender, R., Seitz, S., et al. 2004, *A&A*, 421, 41
- Gehrels, N. 1986, *ApJ*, 303, 336
- Giavalisco, M., Ferguson, H. C., Koekemoer, A. M., et al. 2004, *ApJ*, 600, L93
- Giodini, S., Pierini, D., Finoguenov, A., et al. 2009, *ApJ*, 703, 982
- Gladders, M. D., & Yee, H. K. C. 2000, *AJ*, 120, 2148
- Gobat, R., Rosati, P., Strazzullo, V., et al. 2008, *A&A*, 488, 853
- Graham, A. W., & Worley, C. C. 2008, *MNRAS*, 388, 1708
- Heidt, J., Appenzeller, I., Gabasch, A., et al. 2003, *A&A*, 398, 49
- Hilton, M., Stanford, S. A., Stott, J. P., et al. 2009, *ApJ*, 697, 436
- Hilton, M., Lloyd-Davies, E., Stanford, S. A., et al. 2010, *ApJ*, 718, 133
- Hoaglin, D. C., Mosteller, F., & Tukey, J. W. 1983, *Understanding robust and exploratory data analysis*, Wiley Series in Probability and Mathematical Statistics (New York: Wiley), ed. D. C. Hoaglin, F. Mosteller, & J. W. Tukey
- Holden, B. P., Illingworth, G. D., Franx, M., et al. 2007, *ApJ*, 670, 190
- Hopkins, P. F., Bundy, K., Hernquist, L., Wuyts, S., & Cox, T. J. 2010, *MNRAS*, 401, 1099
- Huang, J.-S., Cowie, L. L., Gardner, J. P., et al. 1997, *ApJ*, 476, 12
- Ilbert, O., Capak, P., Salvato, M., et al. 2009, *ApJ*, 690, 1236
- Jee, M. J., Blakeslee, J. P., Sirianni, M., et al. 2007, *PASP*, 119, 1403
- Jee, M. J., Rosati, P., Ford, H. C., et al. 2009, *ApJ*, 704, 672
- Kinney, A. L., Calzetti, D., Bohlin, R. C., et al. 1996, *ApJ*, 467, 38
- Kodama, T., & Arimoto, N. 1997, *A&A*, 320, 41
- Kodama, T., & Bower, R. 2003, *MNRAS*, 346, 1
- Kodama, T., Tanaka, I., Kajisawa, M., et al. 2007, *MNRAS*, 377, 1717
- Kriek, M., van der Wel, A., van Dokkum, P. G., Franx, M., & Illingworth, G. D. 2008, *ApJ*, 682, 896
- Kroupa, P. 2001, *MNRAS*, 322, 231
- Lidman, C., Rosati, P., Tanaka, M., et al. 2008, *A&A*, 489, 981
- Lin, Y., Mohr, J. J., & Stanford, S. A. 2003, *ApJ*, 591, 749
- Longhetti, M., & Saracco, P. 2009, *MNRAS*, 394, 794
- Longhetti, M., Saracco, P., Severgnini, P., et al. 2007, *MNRAS*, 374, 614
- Madau, P. 1995, *ApJ*, 441, 18
- Maltby, D. T., Aragón-Salamanca, A., Gray, M. E., et al. 2010, *MNRAS*, 402, 282
- Mancini, C., Daddi, E., Renzini, A., et al. 2010, *MNRAS*, 401, 933
- Mancone, C. L., Gonzalez, A. H., Brodwin, M., et al. 2010, *ApJ*, 720, 284
- Mannucci, F., Basile, F., Poggianti, B. M., et al. 2001, *MNRAS*, 326, 745
- Maraston, C. 1998, *MNRAS*, 300, 872
- Maraston, C. 2005, *MNRAS*, 362, 799
- McIntosh, D. H., Bell, E. F., Rix, H., et al. 2005, *ApJ*, 632, 191
- Mei, S., Holden, B. P., Blakeslee, J. P., et al. 2009, *ApJ*, 690, 42
- Menci, N., Rosati, P., Gobat, R., et al. 2008, *ApJ*, 685, 863
- Meurer, G. R., Heckman, T. M., & Calzetti, D. 1999, *ApJ*, 521, 64
- Mullis, C. R., Rosati, P., Lamer, G., et al. 2005, *ApJ*, 623, L85
- Muzzin, A., Wilson, G., Lacy, M., Yee, H. K. C., & Stanford, S. A. 2008, *ApJ*, 686, 966
- Nakata, F., Kajisawa, M., Yamada, T., et al. 2001, *PASJ*, 53, 1139
- Nipoti, C., Treu, T., Auger, M. W., & Bolton, A. S. 2009, *ApJ*, 706, L86
- Nonino, M., Dickinson, M., Rosati, P., et al. 2009, *ApJS*, 183, 244
- Onodera, M., Daddi, E., Gobat, R., et al. 2010, *ApJ*, 715, L6
- Pannella, M., Hopp, U., Saglia, R. P., et al. 2006, *ApJ*, 639, L1
- Pannella, M., Carilli, C. L., Daddi, E., et al. 2009a, *ApJ*, 698, L116
- Pannella, M., Gabasch, A., Goranova, Y., et al. 2009b, *ApJ*, 701, 787
- Papovich, C., Momcheva, I., Willmer, C. N. A., et al. 2010, *ApJ*, 716, 1503
- Peng, C. Y., Ho, L. C., Impey, C. D., & Rix, H. 2002, *AJ*, 124, 266
- Pignatelli, E., Fasano, G., & Cassata, P. 2006, *A&A*, 446, 373
- Postman, M., Franx, M., Cross, N. J. G., et al. 2005, *ApJ*, 623, 721
- Ravindranath, S., Ferguson, H. C., Conselice, C., et al. 2004, *ApJ*, 604, L9
- Ravindranath, S., Giavalisco, M., Ferguson, H. C., et al. 2006, *ApJ*, 652, 963
- Rettura, A., Rosati, P., Strazzullo, V., et al. 2006, *A&A*, 458, 717
- Rettura, A., Rosati, P., Nonino, M., et al. 2010, *ApJ*, 709, 512
- Retzlaff, J., Rosati, P., Dickinson, M., et al. 2010, *A&A*, 511, A50
- Romeo, A. D., Napolitano, N. R., Covone, G., et al. 2008, *MNRAS*, 389, 13
- Rosati, P., Borgani, S., & Norman, C. 2002, *ARA&A*, 40, 539
- Rosati, P., Tozzi, P., Gobat, R., et al. 2009, *A&A*, 508, 583
- Salim, S., Rich, R. M., Charlot, S., et al. 2007, *ApJS*, 173, 267
- Salpeter, E. E. 1955, *ApJ*, 121, 161
- Saracco, P., Longhetti, M., & Gargiulo, A. 2010, *MNRAS*, 408, L21
- Schechter, P. 1976, *ApJ*, 203, 297
- Schlegel, D. J., Finkbeiner, D. P., & Davis, M. 1998, *ApJ*, 500, 525
- Seibert, M., Martin, D. C., Heckman, T. M., et al. 2005, *ApJ*, 619, L55
- Sersic, J. L. 1968, *Atlas de galaxias australes* (Cordoba, Argentina: Observatorio Astronomico)
- Shen, S., Mo, H. J., White, S. D. M., et al. 2003, *MNRAS*, 343, 978
- Stanford, S. A., Eisenhardt, P. R., Brodwin, M., et al. 2005, *ApJ*, 634, L129
- Stanford, S. A., Romer, A. K., Sabirli, K., et al. 2006, *ApJ*, 646, L13
- Staniszewski, Z., Ade, P. A. R., Air, K. A., et al. 2009, *ApJ*, 701, 32
- Stott, J. P., Collins, C. A., Sahlén, M., et al. 2010, *ApJ*, 718, 23
- Strazzullo, V., Rosati, P., Stanford, S. A., et al. 2006, *A&A*, 450, 909
- Szomoru, D., Franx, M., van Dokkum, P. G., et al. 2010, *ApJ*, 714, L244
- Tanaka, M., Finoguenov, A., & Ueda, Y. 2010, *ApJ*, 716, L152
- Taylor, E. N., Franx, M., Glazebrook, K., et al. 2010, *ApJ*, 720, 723
- Thompson, R. I., Illingworth, G., Bouwens, R., et al. 2005, *AJ*, 130, 1
- Toft, S., Mainieri, V., Rosati, P., et al. 2004, *A&A*, 422, 29
- Toft, S., Soucail, G., & Hjorth, J. 2003, *MNRAS*, 344, 337
- Tran, K., Papovich, C., Saintonge, A., et al. 2010, *ApJ*, 719, L126
- Trujillo, I., Feulner, G., Goranova, Y., et al. 2006a, *MNRAS*, 373, L36
- Trujillo, I., Förster Schreiber, N. M., Rudnick, G., et al. 2006b, *ApJ*, 650, 18
- Trujillo, I., Conselice, C. J., Bundy, K., et al. 2007, *MNRAS*, 382, 109
- Valentinuzzi, T., Fritz, J., Poggianti, B. M., et al. 2010, *ApJ*, 712, 226
- van der Wel, A., Holden, B. P., Zirm, A. W., et al. 2008, *ApJ*, 688, 48
- van der Wel, A., Bell, E. F., van den Bosch, F. C., Gallazzi, A., & Rix, H. 2009, *ApJ*, 698, 1232
- von der Linden, A., Best, P. N., Kauffmann, G., & White, S. D. M. 2007, *MNRAS*, 379, 867
- Williams, R. E., Blacker, B., Dickinson, M., et al. 1996, *AJ*, 112, 1335
- Williams, R. J., Quadri, R. F., Franx, M., et al. 2010, *ApJ*, 713, 738
- Wilson, G., Muzzin, A., Lacy, M., et al. 2005, *BAAS*, 37, 1485
- Wilson, G., Muzzin, A., Yee, H. K. C., et al. 2009, *ApJ*, 698, 1943
- Wittman, D., Dell'Antonio, I. P., Hughes, J. P., et al. 2006, *ApJ*, 643, 128
- Yan, R., Newman, J. A., Faber, S. M., et al. 2006, *ApJ*, 648, 281
- Zirm, A. W., Stanford, S. A., Postman, M., et al. 2008, *ApJ*, 680, 224